Earth and Planetary Science Letters 599 (2022) 117836

Contents lists available at ScienceDirect

Earth and Planetary Science Letters

www.elsevier.com/locate/epsl

Sulfur recycling in subduction zones and the oxygen fugacity of mafic arc magmas

Michelle J. Muth [a,b,*], Paul J. Wallace [a]

[a] Department of Earth Sciences, University of Oregon, OR 97403, USA
[b] Department of Mineral Sciences, National Museum of Natural History, Smithsonian Institution, Washington DC 20560, USA

ARTICLE INFO

Article history:
Received 13 December 2021
Received in revised form 21 September 2022
Accepted 21 September 2022
Available online 18 October 2022
Editor: R. Hickey-Vargas

Keywords:
subduction zones
volatiles
sulfur
arc magmas
melt inclusions
basalts

ABSTRACT

Sulfur is important to a range of subduction zone processes, but the factors controlling the sulfur content of primitive arc magmas are poorly understood. In particular, uncertainties about the oxidation state of primary melts in the sub-arc mantle hinder efforts to understand the behavior of sulfur in arc magmas. Here, we use olivine-hosted melt inclusion data from 32 arc segments globally to characterize sulfur contents of magmas from a variety of subduction zones and identify the key processes that control the sulfur content of arc magmas. Average primary magma sulfur contents estimated from these data range from 466 ± 220 ppm (Mariana Forearc) to 4,264 ± 819 ppm (Ecuador). Primitive and more evolved magmas in both hot- and cold-slab subduction zones commonly have higher sulfur contents than mid-ocean ridge basalt (MORB) magmas. In most cases, these elevated sulfur contents require a subduction-modified mantle source with more sulfur than MORB-source mantle. Correlations between magma S and Cl concentrations and S/Dy and Th/Yb ratios in the global data set confirm that sulfur is partially sourced from the subducting slab. By comparing melt inclusion sulfur contents to sulfur solubility limits imposed by sulfide saturation, we find that 88% of arc magmas in our compilation require conditions more oxidizing than the quartz-fayalite-magnetite buffer (QFM). The relationship between S/Dy and calculated magmatic oxygen fugacity (f_{O2}) suggests that slab-derived sulfate is responsible for the higher oxidation state of arc magmas compared to MORB. Model calculations of redox equilibrium between S and Fe species in basaltic melts when sulfate is added to the mantle wedge demonstrate the feasibility of this causal link, which can explain the common range of arc magma f_{O2} values observed for subduction zones globally. Correlations between magma sulfur contents, f_{O2}, and the proportion of added slab-derived material inferred from trace elements can drive associations between high Sr/Y magmas and fertile porphyry ore deposits, as well as the MORB-like Cu contents of arc magmas.

1. Introduction

Globally, many arc magmas have sulfur contents that are elevated relative to mid-ocean ridge basalts (MORB; Wallace and Edmonds, 2011), which suggests that subduction processes play an important role in controlling the sulfur content of arc magmas. However, the processes linking subduction and elevated magma sulfur contents are unclear. Sulfur enters subduction zones via the subducting plate and is present in seafloor sediments, unaltered and hydrothermally altered oceanic crust (Alt and Burdett, 1992; Alt, 1995), and serpentinized lithospheric mantle (Alt et al., 2013). Sulfur is also present in sub-arc mantle wedge peridotite (mostly in sulfide phases) before any subduction-related enrichment (Lorand and Luguet, 2016). The variety of sources, multiple possible valence states (S^{2-}, S^{-}, S^{4+}, S^{6+}), and partitioning between different phases (silicate melt, sulfide, aqueous fluid), all lead to a complexity of pathways that sulfur can take between subduction and eruption. This complexity affects the behavior of many ore-forming metals (Richards, 2015; Park et al., 2021), the long-term redox budget of Earth's mantle (Evans, 2012), and the degassing of SO_2 that is commonly used to monitor volcanic activity (de Moor et al., 2013).

The sulfur contents of primary arc magmas are sensitive to three key factors. One is the sulfur content of the mantle source prior to any input from slab-derived materials. The mantle source beneath arcs is variable in isotopic and trace element composition, ranging from depleted, MORB-like mantle sources to those more similar to the source of ocean island basalts (Pearce and Peate, 1995; Turner and Langmuir, 2022). The processes that formed

* Corresponding author at: Department of Mineral Sciences, National Museum of Natural History, Smithsonian Institution, Washington DC 20560, USA.
E-mail address: muthm@si.edu (M.J. Muth).

https://doi.org/10.1016/j.epsl.2022.117836
0012-821X/

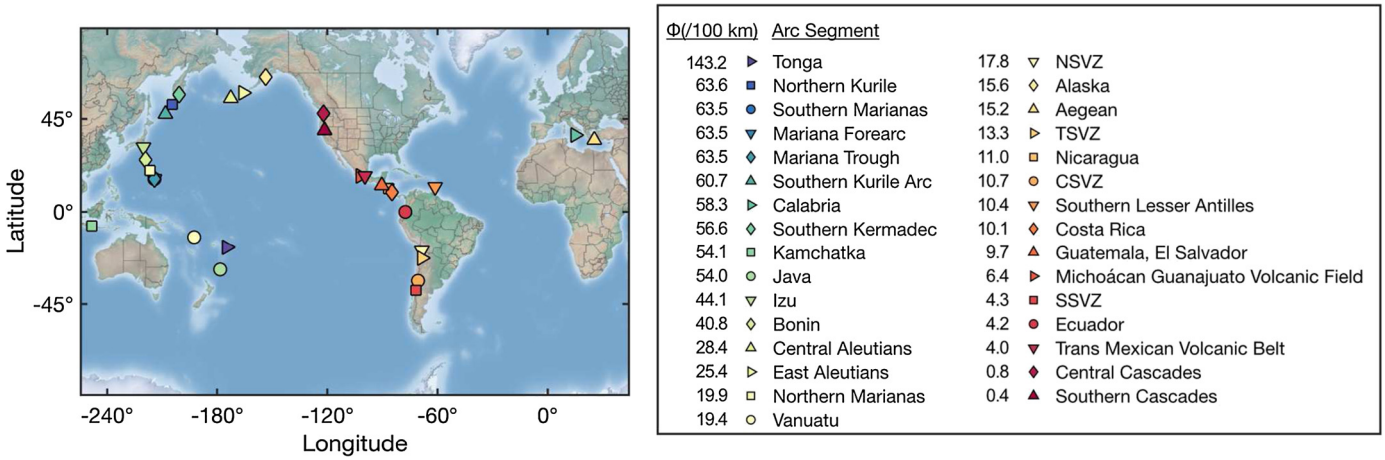

Fig. 1. Map showing the locations of arc segments studied here. Each symbol represents the location of a given arc segment. Arc segments ordered and colored according to slab thermal parameter (Φ, Syracuse et al., 2010), are listed to the left of each symbol label. (For interpretation of the colors in the figure(s), the reader is referred to the web version of this article.) NSVZ, TSZV, CSVZ, and SSVZ represent Northern, Transitional, Central and Southern Southern Volcanic Zone, respectively.

these ambient mantle heterogeneities likely also created variations in the sulfur content of the sub-arc mantle.

The second factor is the mass addition of slab-derived material into the mantle source of arc magmas. Experimental evidence suggests that slab-derived melts and fluids can transfer significant amounts of sulfur into the mantle wedge (Jégo and Dasgupta, 2014). Sulfur isotope variations in high pressure serpentinites and metabasalts also suggest sulfur mobility during progressive dehydration of subducting slabs (Walters et al., 2019; and references therein) although estimates for the degree of mobility vary (Li et al., 2020).

The third factor is oxidation state during mantle melting. Globally, arc magmas and their mantle sources are oxidized relative to mid-ocean ridge basalts (Cottrell et al., 2021), and measured $Fe^{3+}/\Sigma Fe$ values in silicate glasses (Kelley and Cottrell, 2009; Brounce et al., 2021) suggest that the mantle source for arc magmas is oxidized by the input of slab-derived materials to the mantle wedge. Increases in the oxidation state of the mantle wedge affect sulfur solubility in silicate melts during mantle melting, driving enrichments in the sulfur contents of primary magmas (Jugo et al., 2010; Mironov and Portnyagin, 2018; Chowdhury and Dasgupta, 2019; Muth and Wallace, 2021; Xu and Li, 2021).

Importantly, these last two factors are almost certainly linked, with addition of slab-derived material causing an increase in the oxidation state of subduction modified mantle. Combined geochemical and geodynamic models predict the transport of oxidized sulfur into the mantle wedge in slab-derived silicate melts (Canil and Fellows, 2017) or fluids (Tomkins and Evans, 2015; Walters et al., 2020), though these predictions require that the subducting slab is oxidized, which has been debated (e.g. Evans and Frost, 2021; and references therein). The presence of oxidized sulfur in the slab component can increase the oxygen fugacity of the modified mantle wedge and the melts that form within it (Evans, 2012; Muth and Wallace, 2021).

The challenge is to unravel how strongly each of these three factors – mantle heterogeneity, slab-derived sulfur, mantle oxidation state – influence the sulfur content of arc magmas. A major obstacle to doing this is that sulfur, like other volatile elements, is lost to the gas phase during the shallow storage and eruption of arc magmas. There are several ways to work around this challenge. One method is to use the partitioning behavior of chalcophile elements such as Cu to track the behavior of sulfur indirectly (Lee et al., 2012; Barber et al., 2021; Zhang et al., 2021; Zhao et al., 2022). This approach has the advantage of relying less on finding undegassed arc samples. However, while this method is extremely sensitive to the stability of sulfides, it cannot directly constrain the amount of sulfur dissolved in silicate melts. Direct measurements of sulfur isotope ratios in submarine glasses, volcanic gas, and whole rock samples provide valuable information about the sources of sulfur in subduction zones, but sulfur contents in most of these samples have been affected by partial or complete degassing (e.g. de Moor et al., 2021; and references therein).

Melt inclusions allow direct determination of sulfur concentrations in arc magmas, making them an excellent complement to other approaches. Melt inclusions are tiny parcels of silicate melt trapped in phenocrysts. When trapped at sufficiently high pressure, the melts are unaffected or only minimally affected by sulfur loss to degassing. Measuring the sulfur contents and major element compositions of melt inclusions in relatively Mg-rich olivine allows one to estimate the sulfur content of primitive arc magmas (Wallace and Edmonds, 2011; Muth and Wallace, 2021; Zelenski et al., 2022). In this study, we combine measured sulfur contents of melt inclusions with major and trace elements to constrain the sulfur content of the mantle source for subduction zone magmas, the characteristics of slab-derived sulfur in arc magmas, and the oxygen fugacity during mantle melting needed to generate the sulfur content observed at each arc. To investigate the global-scale controls on arc magmatic sulfur, we compiled published melt inclusion datasets from 140 volcanoes in 32 subduction zone segments (Fig. 1).

2. Methods

To compile compositions of the most primitive, least-degassed arc melts, we used olivine-hosted melt inclusions (MI), because olivine is the liquidus phase (+Cr-spinel) in most arc magmas. To take advantage of all available data and assess a full range of subduction-related processes, we included both arc front and non-arc front volcanoes. To compare volcanoes between different subduction zones, we group volcanoes into arc segments with distinct slab thermal parameters (Φ) as reported in Syracuse et al. (2010). Slab thermal parameter is the product of plate age, plate convergence velocity, and the sine of the slab dip angle (Syracuse et al., 2010; and references therein). Although slab thermal parameter is a simplistic measure of slab thermal regime, we use it here to make broad comparisons across subduction zones and note that comparisons using more complex formulations are similar to those being made here (Fig. S1).

Because melt inclusion data are not as widely available as whole rock data, and certain arcs have been better studied than

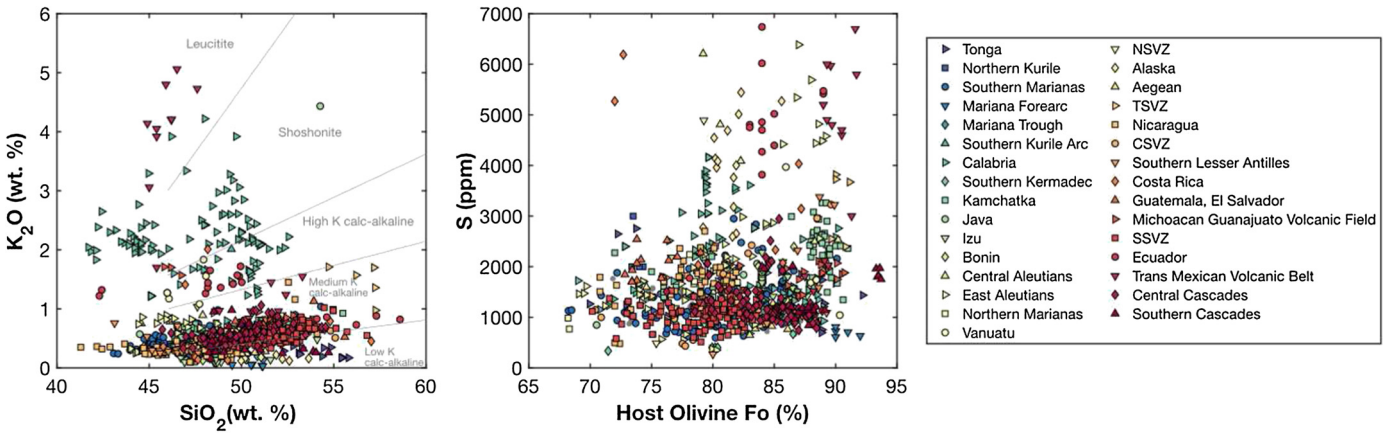

Fig. 2. PEC-corrected compositions of compiled melt inclusions. Each symbol represents one melt inclusion. Each symbol type represents one subduction zone segment. Gray symbols in the panel on the right show MORB glass data (Jenner and O'Neil, 2012), with calculated equilibrium olivine compositions using olivine-melt models as described in the supplemental text. Although many arc melt inclusion sulfur contents are similar to MORB glasses, arc melt inclusions often have lower FeO^T (Fig. S3) and crystallize at lower temperatures due to the effect of H_2O on the olivine liquidus (Médard and Grove, 2008). These factors decrease the sulfur content at sulfide saturation ($SCSS^T$) at a given olivine forsterite composition and magmatic f_{O2} value.

others, the distribution of data across different arcs is uneven. Intermediate to colder slab arcs such as those in the SW Pacific have less available melt inclusion data than intermediate to warmer slab arcs such as the Cascades and Central America. To mitigate the effects of this sampling bias in our interpretations, we present data as both individual volcano/melt inclusion data and as averages for each arc.

We used MI compositions that had been screened for and corrected (when necessary) for effects of post-entrapment crystallization (PEC) and Fe-Mg re-equilibration by the original authors. There are several sources of uncertainty that affect the data and interpretations presented here, including analytical errors and the potential influence of sulfur degassing and sulfide precipitation. The steps we took to mitigate those uncertainties are described in the Supplementary Information. The effect of each of these uncertainties would be to skew the data toward lower sulfur values, and thus our data set provides a robust lower limit to primitive melt sulfur contents for arc magmas.

To consider the behavior of sulfur during mantle melting and to make direct comparisons between melt inclusions trapped during different stages of crystallization, we calculate a primary magma composition for each volcano in each arc segment. For each MI from the upper quartile of S/K_2O values at each volcano, we use reverse crystallization models to calculate melts in equilibrium with Fo_{90} olivine, which is assumed to be the mantle olivine composition (Fig. S2). See Supplementary Information for model details. If the H_2O contents of MI were not reported, we used the average H_2O content of other melt inclusions from the same volcano, or if this information is not available, from the same arc segment. We make the additional assumption that olivine has dominated the crystallization behavior at each volcano. This is consistent with the lack of any clear Al_2O_3 depletions in the data set from each volcano, although some more evolved (lower MgO) MI show scattered Al_2O_3 trends that may indicate some plagioclase fractionation. To calculate the S, Cl, and trace element concentrations for primary magmas from each volcano, we assume that these elements are perfectly incompatible during crystallization, and we dilute each according to the percent K_2O dilution from the calculations above (Fig. S2). Because magmas may undergo some degree of sulfide precipitation and/or sulfur degassing prior to inclusion entrapment, we again emphasize that the primary magma sulfur contents calculated here are minimum estimates.

3. Results

The final filtered data set contains data from 919 melt inclusions. The data set spans 32 arc segments and 140 volcanoes. Most inclusions are low to medium-K calc-alkaline basalt or basaltic andesite (Fig. 2). Average PEC-corrected MI sulfur contents for each arc segment range from 594 ± 241 ppm (Mariana Forearc) to $5{,}022 \pm 795$ ppm (Ecuador; Fig. 2). Average calculated primary magma sulfur contents for each arc range from 466 ± 220 ppm to $4{,}264 \pm 819$ ppm (Fig. 3). Sulfur contents are elevated relative to those measured in mid-ocean ridge basalts, across a range of both host olivine forsterite content (Fig. 2) and subduction zone slab thermal parameter (Fig. 3). Importantly, the full global range of sulfur concentrations occurs in olivine hosts with Fo_{88-92} composition, demonstrating the highly variable sulfur contents of primitive arc melts.

4. Discussion

4.1. Controls on the sulfur contents of arc magmas

There are three key controls on the sulfur content of primary arc magmas. The first is the composition of the mantle wedge source before any addition of slab-derived components. For example, removal of sulfur from the mantle source during previous melting episodes would leave the mantle depleted in sulfur compared to more fertile mantle sources. The second factor is the addition of slab-derived sulfur to the mantle wedge by aqueous fluid, hydrous silicate melt, and/or a supercritical phase. The third factor is the oxygen fugacity during mantle melting, which strongly influences mantle sulfide saturation. If the mantle is saturated in sulfide during melting, this will limit the sulfur content of the melt at the total dissolved sulfur content at sulfide saturation ($SCSS^T$). Because $SCSS^T$ is strongly controlled by f_{O2} at the intermediate f_{O2} values typical for arc magmas (Jugo et al., 2010), the sulfur contents of arc magmas are likely to be sensitive to oxidation state during mantle wedge melting.

A first step towards investigating the importance of each control listed above is to determine whether primary arc magmas require elevated sulfur contents in their mantle sources. This is a complex question because the "source" is likely a hybrid of mantle wedge peridotite and slab components, and the latter could be introduced either at some earlier time (metasomatism) or in conjunction with and as the causative force for mantle wedge melting. As a first step, we use simple batch melting models to

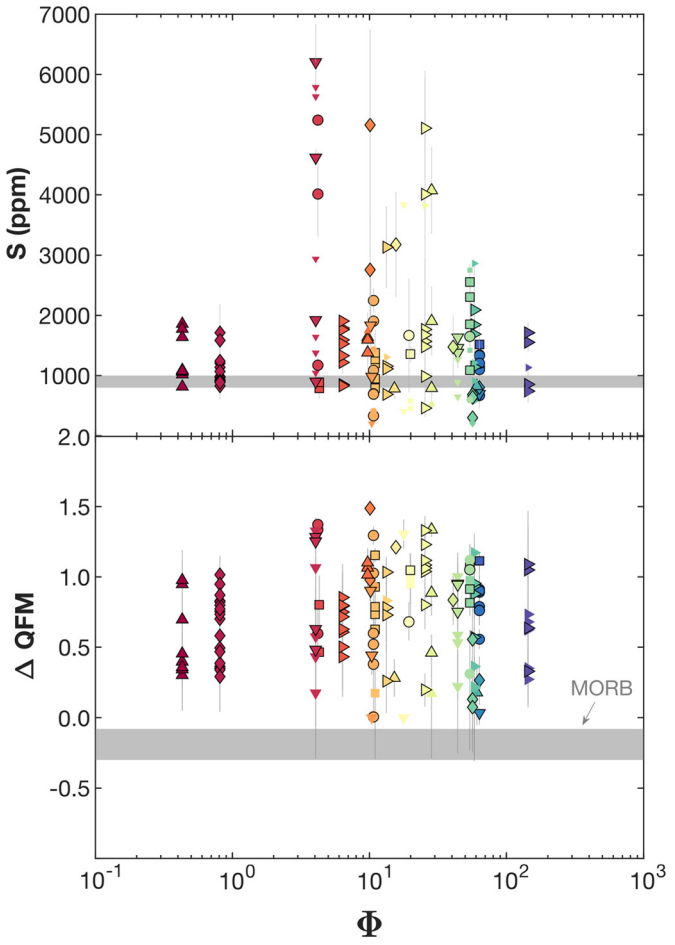

Fig. 3. (Top) Primary magma S concentrations for volcanoes plotted as a function of slab thermal parameter (Φ). Error bars represent uncertainty in primary magma compositions, calculated using the standard deviation of the mean for each volcano data set. Gray bar represents primary MORB S concentrations (Ding and Dasgupta, 2017). (Bottom) Mean minimum relative oxygen fugacity of arc volcano magmas calculated using PEC-corrected melt inclusion sulfur contents at 500 MPa as described in the text. Error bars represent propagated uncertainty. 12% of volcanoes have oxygen fugacity values indistinguishable from MORB and are plotted at QFM = 0 for simplicity. Oxygen fugacity of MORB shown for comparison in gray bar (Zhang et al., 2018). Small symbols represent compositions calculated for volcanoes that had only a single melt inclusion in the upper quartile of their S/K_2O values. Symbols as in Fig. 1.

calculate the minimum mantle sulfur content required to generate primary arc melt sulfur concentrations. As a further simplifying assumption, we assume that the mantle is sulfide-phase free and that sulfur partitioning behavior is instead dominated by silicate minerals. We make this assumption because sulfur behaves more compatibly during sulfide-saturated mantle melting (e.g., Yao et al., 2018). The method used here therefore provides a minimum estimate for source sulfur content. We use partition coefficients from Callegaro et al. (2020) with mineral modal proportions appropriate for spinel lherzolite (Ol:53, Opx:30, Cpx:12, Sp:5). We assume a melt fraction of 15%, consistent with melt fraction estimates for arcs based on trace element concentrations (Pearce and Peate, 1995). These calculations show that arc magmas require minimum mantle source sulfur contents ranging from 31 to 1011 ppm sulfur (Fig. S4). Varying melt fraction to 10 and 20% shifts this range to 21–676 ppm S and 40–1345 ppm S, respectively. In comparison, estimates for MORB-source mantle are 100–200 ppm S (Ding and Dasgupta, 2017; Sun et al., 2020; and references therein). These results indicate that any model used to explain the sulfur contents of arc magmas globally must involve source (mantle plus added slab components) sulfur contents that are higher in many cases than those in the MORB source. In the following sections, we discuss the effects of mantle wedge composition, addition of slab components, and mantle oxidation state in controlling the sulfur content of primary arc magmas.

4.1.1. Mantle source

One important control on arc magma sulfur contents is the initial sulfur budget of the mantle prior to addition of slab components. We recognize, however, that for relatively long-lived arc systems, there may be a long history involving multiple episodes of both slab addition and melt extraction, making it difficult to distinguish a 'pre-subduction' mantle wedge source. It has been estimated that the sulfur contents of E-DMM and D-DMM (enriched and depleted mantle, respectively, compared to average depleted MORB mantle) vary from 165 to 100 ppm (Shimizu et al., 2016). Ocean island basalt (OIB) sulfur and copper systematics suggest the sulfur content of OIB mantle sources are variable and commonly lower than this range (Ding and Dasgupta, 2018). Many magmas in continental arcs show evidence of an enriched component in the mantle wedge, perhaps due to the incorporation of components of subcontinental lithospheric mantle within the asthenospheric mantle source (Turner and Langmuir, 2022; and references therein). In contrast, the mantle sources for island arcs are commonly more depleted than those of continental arcs, and in some cases are even more depleted than DMM (e.g. Pearce and Peate, 1995). As discussed in previous global arc studies (Turner and Langmuir, 2022; and references therein) arcs where the subducted plate has a higher thermal parameter (colder slabs) generally have thinner, oceanic overlying crust, whereas arcs with lower thermal parameter (hotter slab) generally have thicker, continental overlying crust (Fig. S5). This association means that distinguishing between variations in arc geochemistry caused by differences in slab thermal state, crustal thickness, and mantle composition is an important part of interpreting global arc data sets.

Because sulfur is dominantly hosted in sulfide phases in mantle peridotite and not in silicate minerals (Lorand and Luguet, 2016; Yao et al., 2018; Callegaro et al., 2020), mantle sulfur concentration can become decoupled from rare earth element (REE) enrichment/depletion trends. In extreme cases, chalcophile element depletions have been linked to melt percolation events with high melt/rock ratios that destabilize mantle sulfides (Lorand and Luguet, 2016). However, mantle peridotites generally show positive correlations between peridotite fertility indices (such as Al_2O_3) and S and Cu concentrations, suggesting that the sulfur content of peridotites is dominantly controlled by previous melting events (Lorand and Luguet, 2016), which are in turn influenced by parameters such as mantle wedge temperature and oxidation state (Yao et al., 2018).

To investigate whether variations in arc magma sulfur content are related to heterogeneity in the sub-arc mantle source prior to subduction influence, we compare Nb/Y to S/Dy (Fig. 4). Ratios such as Nb/Y that compare two elements with different degrees of incompatibility are useful indicators of the extent of depletion of the mantle by previous melt extraction or involvement of an enriched component as described above (e.g., Pearce and Peate, 1995). High S/Dy values indicate increases in the sulfur content of magmas due to higher concentrations of sulfur in the mantle source and/or more oxidized melting conditions (e.g., Muth and Wallace, 2021).

While the lack of clear Al_2O_3 depletion trends in individual melt inclusion data sets suggest the influence of plagioclase crystallization is small, some more evolved compositions show CaO depletions consistent with clinopyroxene and/or amphibole crystallization, both of which could influence S/Dy values. For example, assuming fractional crystallization and using partition coefficients from Green (1994), and Callegaro et al. (2020), 50% crystalliza-

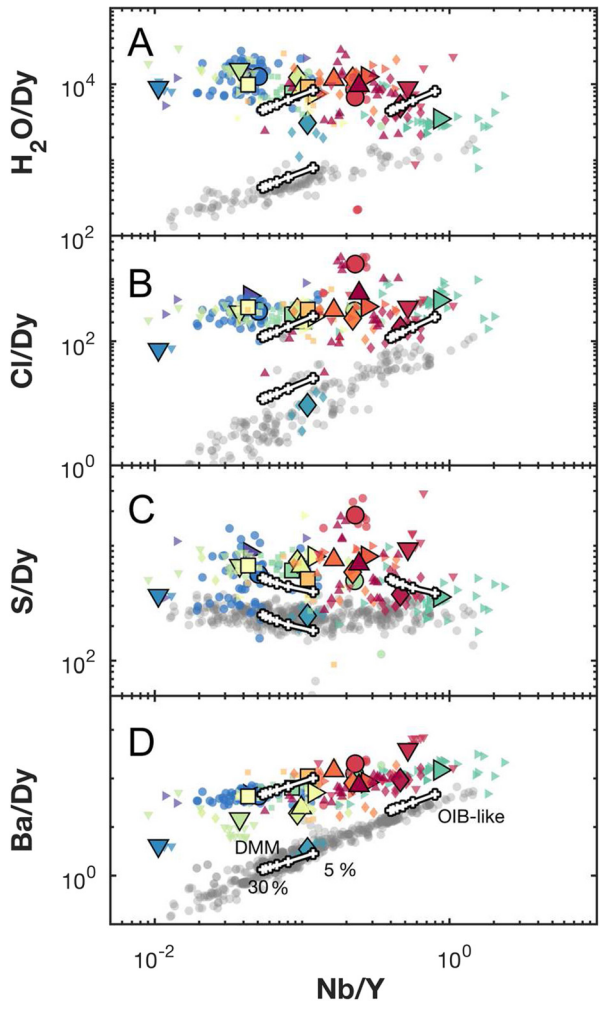

Fig. 4. Melt inclusion compositions of volcanoes within each arc segment. Each small symbol represents one analyzed inclusion, and large symbols represent the average value for each arc. Symbol types as in Fig. 1. Small gray symbols are MORB compositions (Jenner and O'Neil, 2012; Shimizu et al., 2016; Le Voyer et al., 2019). MORB Cl contents were filtered (Cl/K < 0.08) to exclude those affected by assimilation involving a seawater-derived component. Three batch melting curves are shown for comparison. The first is based on DMM for trace elements and Pacific Upper Plate source for volatile elements. The second contains 300 ppm S, 50 ppm Cl, 2000 ppm H_2O, and 20 ppm Ba. Nb, Y, and Dy concentrations are the same as DMM. The third is an enriched mantle source composition estimated for the Central Oregon Cascades and volatile and Ba contents based on the same volatile-enriched DMM mantle source used for the second curve described above. References for each source composition and partition coefficient are listed in supplemental material. Tick marks on each model curve represent percent melt fraction, as shown in the lowermost panel.

tion of a clinopyroxene-bearing assemblage (half olivine and half clinopyroxene), or amphibole-bearing assemblage (half olivine and half amphibole), would change an original S/Dy value of 273 to 331 and 359, respectively. In contrast, 50% crystallization of olivine only would only change S/Dy to 271. While it is difficult to rule out these effects definitively, the changes in S/Dy described above are small relative to the total range of S/Dy values in our data set (92-2601). Furthermore, comparisons of S/Dy trends between arcs broadly mirror those in sulfur concentration and show no systematic changes with host-olivine forsterite content (Fig. S6). We therefore conclude that the effects of crystallization on S/Dy are secondary and attribute variations in S/Dy within our data set primarily to variability in the compositions of primary arc magmas.

S/Dy ratios in arc magmas are almost all higher than MORB, whereas Nb/Y contents of arc magmas span the range of values observed in MORB (Fig. 4). Consistent with previous work as discussed above, intra-oceanic arcs, which tend to overlie colder subducting slabs, commonly have more depleted mantle sources, whereas continental arcs, which tend to overlie hotter subducting slabs, commonly have more enriched mantle sources. We do note the exception, however, that one cold-slab arc (Calabria) has the most enriched mantle composition of the entire global array. This exception may be related to the complex geodynamic regime in the region (De Astis et al., 2003). Comparing the different arcs, Cl/Dy, H_2O/Dy, and Ba/Dy are more elevated relative to the MORB array in colder-slab arcs with more depleted mantle sources. This link is likely due to the overall association between colder slabs and the more depleted mantle common in intra-oceanic arcs, such that the effect of added slab components on magmatic Cl, H_2O, and Ba contents is more pronounced (Fig. S5; Ruscitto et al., 2012). Within arc variations in these elements can therefore largely be explained by variations in melt fraction and slab-component addition superimposed on small variability in source composition. In contrast, for S/Dy, there is more overlap at the low end of arc values with the MORB field, consistent with the interpretation that sulfur is more equally sourced from mantle wedge and slab components compared to Cl, H_2O, and Ba, which are dominated more by slab inputs. Comparing different arcs, there are no systematic variations between S/Dy and Nb/Y, indicating that sulfur enrichment in arc magmas is not dominantly controlled by prior enrichment or depletion of the mantle source.

4.1.2. Slab-derived materials

Here we investigate the role of mass transfer of sulfur from the subducting slab into the overlying mantle wedge in controlling the sulfur content of arc magmas. There is strong evidence for slab-derived mass transfer of sulfur in the ^{34}S-rich sulfur commonly measured in arc glasses and volcanic gases (Bénard et al., 2018; Muth and Wallace, 2021; de Moor et al., 2021; and references therein), which suggest the input of ^{34}S-rich seawater-derived sulfur in the sulfur budget of arc magmas. Experiments and thermodynamic models also indicate that slab-derived melts and fluids can carry a significant amount of sulfur (Jégo and Dasgupta, 2014; Tomkins and Evans, 2015; Walters et al., 2020).

One way to assess the mass transfer of sulfur is by comparing sulfur to chlorine. Chlorine is elevated in arc magmas relative to MORB and is derived from the subducting slab (Ruscitto et al., 2012). This comparison is valuable because chlorine is very soluble in basaltic melts and degasses strongly only at relatively low (< 100 MPa) pressure, in contrast to sulfur, which may be lost to degassing or to sulfide formation, especially in more evolved magmas (Wallace and Edmonds, 2011; and references therein). Chlorine also has straightforward melting behavior in the mantle, and enrichments in chlorine have been demonstrably linked to slab inputs beneath arcs and back-arcs (Ruscitto et al., 2012; and references therein). Primary magma sulfur and chlorine estimates for arc magmas correlate both within and across arcs, although there is considerable scatter ($R^2 = 0.27$, p-value $= 3.9 \times 10^{-10}$; Fig. 5). Many of the volcanoes with the lowest S/Cl values have atypical melt compositions: high-Mg andesites (Mt. Shasta), nepheline normative (Puñalica), or high-K to shoshonitic (Apaxtepec, Procida Island, Ustica, Aoba Island). In these cases, prior subduction-related metasomatism in the mantle or unusually large proportions of slab-derived materials may create mantle sources with higher concentrations of chlorine.

To investigate the relationship between slab-derived materials and magma sulfur contents more directly, we compare the ratio S/Dy to ΔTh/Yb as an indicator of slab-derived material (Fig. 6). Because ΔTh/Yb tracks increases in Th concentration relative to the MORB array, ΔTh/Yb has the advantage of being relatively independent of mantle source composition compared to more traditional slab-material proxies, which is especially important when

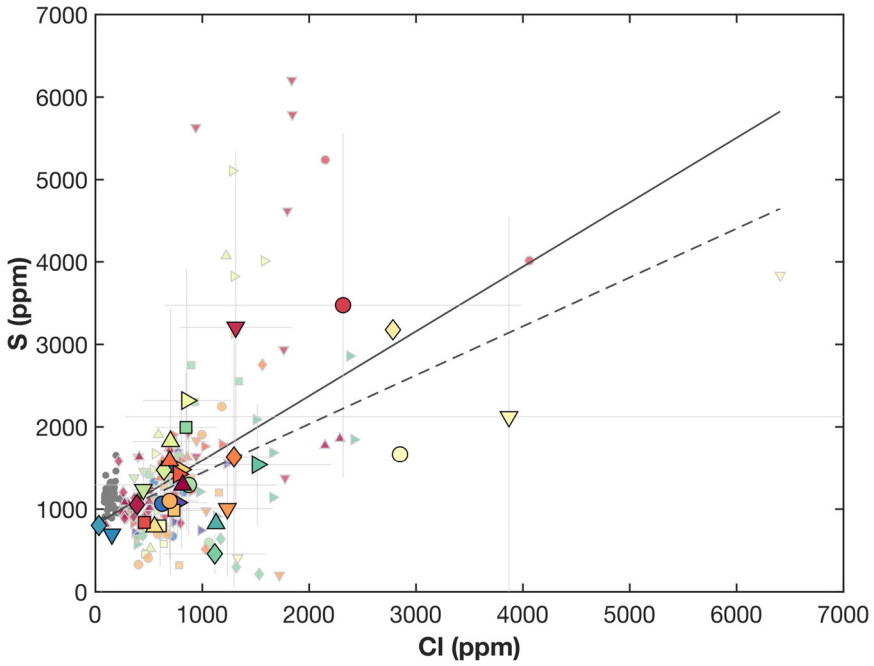

Fig. 5. S and Cl contents of primary magma compositions of volcanoes within each arc. Each small symbol represents one volcano, and large symbols represent the average value for each arc. Error bars represent 2σ standard deviation on calculated arc average. Symbols as in Fig. 1. Small gray symbols are MORB compositions (Cl/K < 0.08) that are unaffected by assimilation involving a seawater-derived component (Jenner and O'Neil, 2012; Shimizu et al., 2016; Le Voyer et al., 2019). Solid line through data shows best fit through all data and dashed line shows best fit excluding atypical compositions as discussed in text.

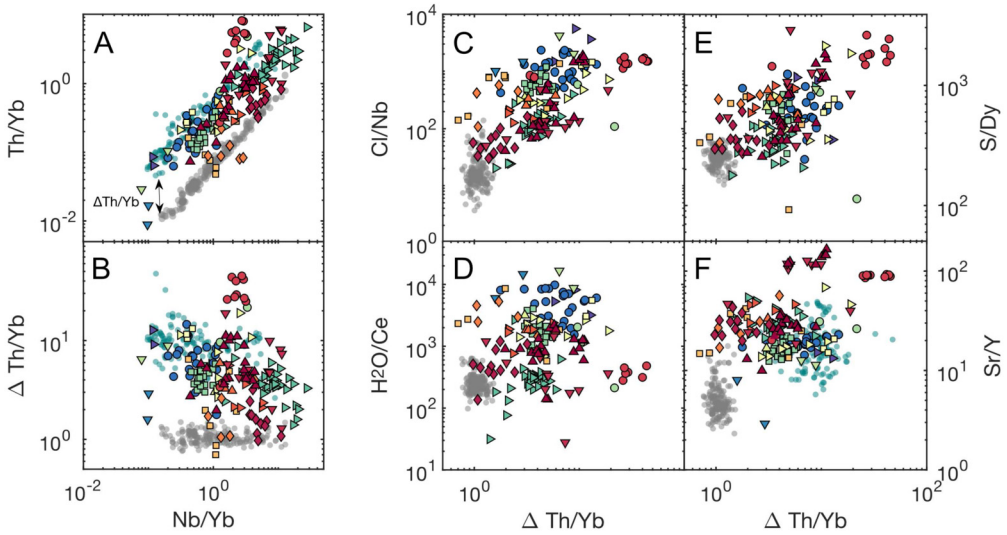

Fig. 6. Primary magma composition for individual melt inclusions from each arc shown in comparison to MORB data (gray circles; Jenner and O'Neil, 2012; Shimizu et al., 2016; Le Voyer et al., 2019) and global arc data (teal circles; Turner and Langmuir, 2022). MORB Cl contents were filtered (Cl/K < 0.08) to exclude those affected by assimilation involving a seawater-derived component. Symbols as in Fig. 1. ΔTh/Yb is defined as the distance to the MORB array in Nb/Yb vs Th/Yb space, where the MORB array is defined via regression.

considering global data sets (Turner and Langmuir, 2022). We note however that arcs with enriched mantle sources still plot to slightly lower ΔTh/Yb values, suggesting the signature of slab-derived Th is dampened slightly by higher ambient mantle Th concentrations. In comparison to the arc-front whole-rock data compilation of Turner and Langmuir (2022), our compilation shows a broader range in ΔTh/Yb values because we include subduction-related volcanoes outside of the main arc axis (e.g. back-arc locales). Although there is considerable scatter, the relationships between S/Dy and Cl/Nb vs. ΔTh/Yb are quite similar. The relationship of H_2O/Ce vs. ΔTh/Yb also clearly shows the effect of slab-derived volatiles, though with some offsets to lower H_2O/Ce values that likely reflect melt inclusions that were affected by post-entrapment diffusive H loss (e.g. BRM in the Southern Cascades; Walowski et al., 2016). In contrast, a comparison of S/Dy and B/Nb (another slab tracer that is influenced by slab thermal structure and dip angle; see Zhang et al., 2021) shows no clear correlation between the two parameters (Fig. S7), but we note that melt inclusion B data are limited.

The patterns discussed above demonstrate that the sulfur content of subduction zone magmas is strongly influenced by slab-derived materials. We explore here whether variations in the amount of slab-derived sulfur are in turn related to the thermal structure of the subducting slab. This exploration is partially motivated by previous comparisons between global arc data and geodynamic models (Ruscitto et al., 2012) which suggested that arcs

with intermediate slab temperatures are most efficient at recycling H_2O. At 6–14 kbar, anhydrite-saturated fluids contain higher sulfur contents at higher temperature (Newton and Manning, 2005). The same relationship has been observed in experiments on slab-derived melts (Jégo and Dasgupta, 2014). However, in our data compilation, the highest primary magma sulfur contents occur in intermediate slab-temperature arcs, not those with the hottest slabs (Fig. 3). Importantly, though, the majority of magma sulfur concentrations for arcs with intermediate temperature slabs overlap with concentrations for arcs with hotter and cooler slabs, suggesting there is no clear relationship between magma sulfur content and the thermal state of the subducting plate. If additional data were to show that higher sulfur contents in arcs with intermediate-temperature slabs was a robust feature, it could indicate that these subduction zones fall in a thermal 'sweet spot', where aqueous fluids, which can dissolve more sulfur than slab melts (Jégo and Dasgupta, 2014), are released simultaneously with slab melts into the mantle wedge (e.g., Ruscitto et al., 2012).

Sulfur speciation in slab-derived fluids and melts may also play a role in driving variations in arc magma sulfur contents. Slab dehydration models that incorporate sulfur predict a release of oxidized sulfur during the blueschist to eclogite transition (Tomkins and Evans, 2015; Walters et al., 2020). Calculations based on anhydrite solubility models (Tomkins and Evans, 2015) and more complex fluid speciation models (Walters et al., 2020) both predict that sulfur released beneath arcs in hot subduction zones is more reduced than sulfur released in cold subduction zones. These differences in sulfur oxidation state likely change the solubility of sulfur in slab melts and fluids and also affect how much dissolved sulfur mantle melts can hold, as discussed in more detail in the section below.

4.1.3. Oxygen fugacity

In addition to the mass transfer of sulfur into the mantle wedge, S/Dy is sensitive to oxidation state during mantle wedge melting, because $SCSS^T$ is extremely sensitive to f_{O2} (Jugo et al., 2010). We can quantify this relationship by calculating a minimum f_{O2} for magmas using the measured sulfur contents in melt inclusions. Under reducing conditions, the $SCSS^T$ is controlled mainly by temperature, pressure, melt FeO^T and H_2O content, and sulfide composition (Smythe et al., 2017; Liu et al., 2021). However, under more oxidizing conditions, where S^{6+} and S^{2-} are both stable, f_{O2} exerts a dominant control (Jugo et al., 2010). The f_{O2} during mantle wedge melting depends on the mineral assemblage and mineral compositions (especially Fe^{3+}/Fe^{2+} ratio) of mantle rock before slab-component addition, as well as the composition of the slab components added. To model the effect of variable f_{O2} on $SCSS^T$, we combine an existing model of the sulfide concentration at sulfide saturation ($SCSS^{2-}$) for reducing conditions (Smythe et al., 2017) with the H_2O effect described in Liu et al. (2021) and an f_{O2} dependence based on 200 MPa experimental data (Fig. 7; Jugo et al., 2010). Although the $SCSS^T$ vs. f_{O2} relationship from Jugo et al. (2010) that we have adopted is based on a limited data set, we note that it is consistent with a recent thermodynamic model (O'Neill and Mavrogenes, 2022). Because $SCSS^T$ and f_{O2} relationships at pressures relevant to mantle melting are less certain (Matjuschkin et al., 2016), we calculate $SCSS^T$ for conditions of crustal storage instead.

This combined model is used to calculate the minimum possible f_{O2} value for each melt inclusion composition by assuming the melt was sulfide saturated during entrapment. At very oxidizing conditions, magmas can also become saturated in anhydrite ($CaSO_4$). However, very few melt inclusions in the current compilation plot close to anhydrite saturation (Fig. S8). For those that may be anhydrite saturated, this method still provides a minimum possible f_{O2}, as magmas that are anhydrite saturated may be even more oxidized than melt sulfur content would indicate based on $SCSS^T$ calculations. In support of our assumption of sulfide saturation at time of trapping, even at higher f_{O2}, we note that a small subset ($\sim$ 2%) of high-Mg melt inclusions from Tolbachik Volcano in Kamchatka contain extremely high sulfur concentrations (4,000–14,000 ppm; Zelenski et al., 2022) and also commonly contain quenched sulfide liquids. This demonstrates that arc magmas may be extremely S rich, even when saturated in a sulfide phase, consistent with experimental results (e.g. Jugo, 2009). We note that these Tolbachik inclusions from Zelenski et al. (2022) are not included in our compilation due to lack of information about the olivine hosts.

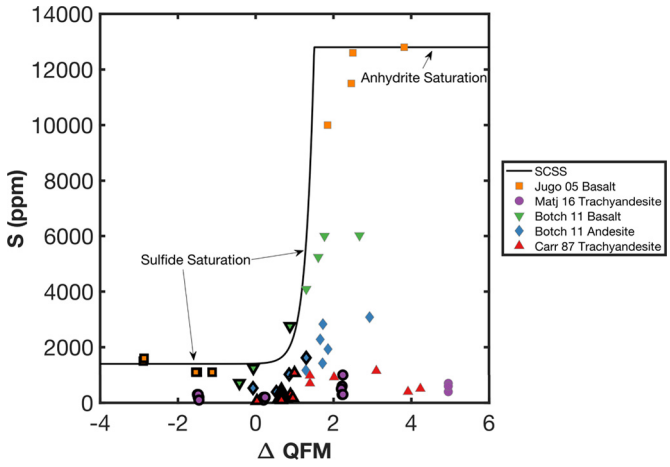

Fig. 7. Sulfur solubility vs. relative oxygen fugacity relationship (black curve; Jugo et al., 2010, 2005) used to calculate the minimum oxygen fugacity required to account for melt inclusion sulfur contents. See text for description of how $SCSS^{2-}$ at lower f_{O2} and $SCSS^T$ at intermediate f_{O2} were calculated for each melt inclusion composition. Measured sulfur contents of experimental glasses of variable melt composition, pressure and temperature are shown for comparison (Jugo et al., 2005; Matjuschkin et al., 2016; Botcharnikov et al., 2011; Carroll and Rutherford, 1987). Thick black outlined symbols are experiments saturated in a sulfide phase. Disequilibrium experiments (not shown) and thermodynamic analysis suggest sulfide is stable up to $\sim$ QFM + 2 (Jugo, 2009).

We calculate the entrapment temperature of melt inclusions by applying the olivine-melt thermometer of Sugawara (2000) combined with the H_2O-dependent term of Médard and Grove (2008) to PEC-corrected melt inclusion compositions and assume 500 MPa pressure. Although 500 MPa is higher than the pressure of the experiments used to calibrate $SCSS^T$ as a function of f_{O2} (200 MPa, Jugo et al., 2010), comparisons to higher pressure experiments (Matjuschkin et al., 2016) indicate that any error introduced by using relationships calibrated for lower pressures would likely cause underestimates in calculated f_{O2}. Therefore, this uncertainty, like the uncertainty in melt sulfur contents (see Supplementary Information), does not undermine our interpretation of these f_{O2} estimates as minimum values. For H_2O content we use either measured H_2O values or average values from the same volcano if melt inclusion H_2O was not measured. We assume $X_{FeS} = 0.85$ in the sulfide phase, consistent with the measured compositions of magmatic sulfides in arc rocks (Georgatou et al., 2018). The 68% confidence interval of the modelled f_{O2} based on these model assumptions was calculated using a Monte Carlo approach for $n = 10{,}000$ iterations. Input parameters were randomly generated assuming a normal distribution and a specified one standard deviation (σ), where $\sigma_T = 100°$, $\sigma_P = 100$ MPa, $\sigma_{H_2O} = 0.5$ wt.%, $\sigma_{XFeS} = 0.1$, $\sigma_S = 15\%$, and $\sigma = 5\%$ for all other major element concentrations used to calculate $SCSS^{2-}$ values for each melt inclusion. This approach assumes the different sources of uncertainty are independent. The error distribution for each melt inclusion composition generated from this calculation was then propagated through the calculation of minimum f_{O2}. During the minimum f_{O2} calcula-

tion, if a given MI sulfur concentration was less than calculated SCSS, f_{O2} was assumed to be QFM. The resulting error distribution for the minimum f_{O2} of each inclusion was also propagated through the mean estimate for each volcano using the Monte Carlo approach for $n = 10{,}000$ iterations.

The results of these calculations show that 88% of arc volcanoes require conditions more oxidizing than QFM (Figs. 3, S9). Minimum f_{O2} estimates calculated with this approach are broadly consistent with f_{O2} calculated using measured $Fe^{3+}/\Sigma Fe$ in melt inclusions (Fig. S10). Degassing, assimilation, and the crystallization of Fe^{2+}-rich phases can all theoretically change the f_{O2} of magmas after mantle melting and before inclusion entrapment. However, arc magma differentiation models indicate that early fractional crystallization drives only modest increases in magma f_{O2} and there is little experimental or natural data to suggest that degassing at depth drives large increases in magma f_{O2} at arcs (Kelley and Cottrell, 2012; Xu and Li, 2021). Although garnet crystallization or more complex magma recharge scenarios can theoretically drive increases in Fe^{3+} (Park et al., 2021; and references therein), such Fe^{3+} increase requires protracted extents of crystallization. However, many of the high-Mg inclusions in the global data compilation have high S contents, inconsistent with a relationship of higher f_{O2} with extent of differentiation (Fig. 2). Furthermore, high melt S contents (Fig. 2) and elevated f_{O2} (Cottrell et al., 2021) are observed in arcs with thin crust, where garnet is unlikely to be stable at depths of crystallization. Assimilation of oxidized crustal material (anhydrite-rich veins or hydrothermally altered rocks) could, in principle, simultaneously cause increases in both sulfur and magma oxidation state (e.g. Chowdhury and Dasgupta, 2019; Zelenski et al., 2022), but it is unlikely this process would occur in the majority of high-Mg melt compositions represented by melt inclusions in the global dataset.

4.2. Slab-derived sulfur and arc magma f_{O2}

The results shown in Fig. 3 suggest a similar range of f_{O2} values for arcs globally, irrespective of slab temperature. The f_{O2} values are broadly consistent with values deduced from other methods (Cottrell et al., 2021, and references therein; Fig. S10), but the lack of correlation with slab temperature contrasts with the results of Zhang et al. (2021) based on Cu contents and V/Yb as f_{O2} proxies. Although our approach and that of Zhang et al. (2021) both have large uncertainties, melt inclusion sulfur contents differ from trace element proxies in that they constrain minimum magmatic f_{O2} independently of mantle source composition. Our work also highlights the variability of S contents in primitive arc magmas, and such variability can influence Cu differentiation trends and therefore affect the use of Cu as a proxy for inferring f_{O2} during mantle melting. The contrasts between our results and those of Zhang et al. (2021) can potentially be reconciled by considering relationships between slab temperature, crustal thickness, and mantle source composition, as detailed in section 4.1.1.

Because mass balance and sulfur isotopic constraints require slab-derived addition of sulfur into the mantle wedge, our results suggest that the addition of sulfur is directly linked to increases in oxygen fugacity during melting. The S/Dy ratio, which increases with the addition of slab S into the melting region and is relatively independent of variations in melt fraction during sulfide-saturated mantle melting, demonstrates the link between added S and increased f_{O2} (Fig. 8). This link has been previously proposed because slab-derived S^{6+} (in hydrous silicate melts or slab-derived aqueous fluids) or S^{4+} (in fluids) are effective oxidizing agents in the mantle wedge (Kelley and Cottrell, 2009; Evans, 2012; Klimm et al., 2012).

A number of slab dehydration and melting models predict the release of oxidized sulfur at sub-arc depths. Thermodynamic models of sulfide-sulfate buffer reactions during the subduction of sediment lithologies suggest that subducted sediments, particularly those in cold arcs, can contain substantial anhydrite at sub-arc depths (Canil and Fellows, 2017). Similarly, thermodynamic models of fluids released from subducting altered oceanic crust indicate that substantial sulfur is released as S^{4+} or S^{6+} at sub-arc depths, although the proportion of oxidized sulfur species depends on the degree of oceanic crust alteration before subduction and the thermal structure of the subduction zone (Walters et al., 2020). Forward models of fluids released from hydrated mantle lithosphere in subducting slabs predict a range of sulfur speciation depending primarily on assumptions about the initial composition and oxidation state of the downgoing serpentinite. This highlights the need for a more detailed understanding of serpentinite composition and P-T conditions within subducting slabs (Evans and Frost, 2021). Petrologic observations and reactive transport models also indicate that slab sediments may act as an 'oxidative filter' and oxidize more reduced fluids that pass through the sediments from deeper in the slab (Ague et al., 2022).

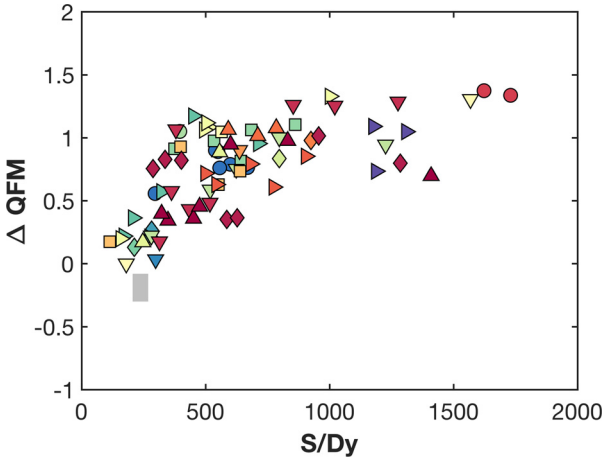

Fig. 8. Mean calculated minimum f_{O2} based on sulfur contents of melt inclusions, plotted as a function of primary magma S/Dy for volcanos from each arc segment. Symbols as in Fig. 1. Gray box bounds the upper and lower quartile values for MORB (Zhang et al., 2018; Jenner and O'Neil, 2012). It should be noted that the ΔQFM values are calculated from melt inclusion S and major element composition, as described in the text, causing an inherent correlation between the parameters shown here. However, increase in S/Dy relative to MORB values requires addition of slab-derived S, and thus the pattern shown here must reflect increases in f_{O2} that are correlated with S addition.

From a 'top down' perspective, oxidizing, S^{6+} rich slab-derived fluids are consistent with evidence that elevated magma f_{O2} is directly linked to slab-derived material in the Mariana Arc (Kelley and Cottrell, 2009, 2012; Brounce et al., 2021), and that slab-derived S^{6+} in the Cascade Arc is linked to elevated magma f_{O2} (Muth and Wallace, 2021). Many arc magmas are also enriched in ^{34}S relative to MORB, consistent with either the direct transfer of seawater-derived sulfate from the slab into the sub-arc mantle source or isotopic fractionation between sulfide-bearing slab lithologies and S^{6+}-rich fluids or melts (Bénard et al., 2018; Muth and Wallace, 2021; and references therein). ^{34}S-enriched arc magmas could also result from reactive transport and partial reduction of sulfur as fluids migrate within slab lithologies (Walters et al., 2019). The somewhat restricted range of observed arc magma $\delta^{34}S$ values (Muth and Wallace, 2021) suggests that if open-system fractionation does occur, its extent is relatively limited in affecting slab components that reach the sub-arc mantle wedge.

Slab-derived S^{6+} can be an effective oxidizing agent in the mantle wedge, but its effect is muted to some extent by interaction with the high concentrations of Fe^{2+} in mantle wedge peridotite. The implications of this interaction between slab S^{6+} and mantle Fe^{2+} depend partially on whether the mantle goes through one

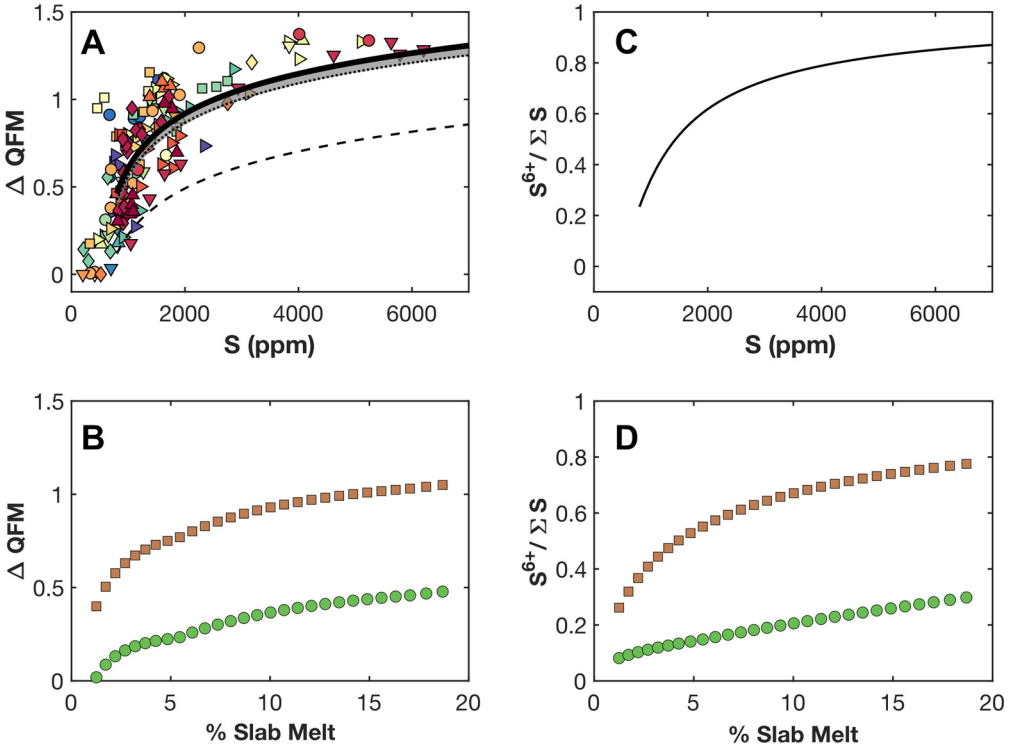

Fig. 9. (A) Mean minimum f_{O2} calculated for magmas at each volcano shown as a function of primary magma sulfur content. The black line shows the effect of S^{6+} titration into N-MORB composition at 1150 °C as described in the text for oxygen fugacity (A) and sulfur valence state (B). The gray field bounds the calculation at 1050 °C and 1250 °C. Dotted curves show calculation using the model of Nash et al. (2019; short dashes) and O'Neill (2021; long dashes) at 1150 °C. (Panels B and D) Calculated oxygen fugacity of mantle melts and $S^{6+}/\Sigma S$ at peak mantle wedge temperature with variable proportions of slab melt containing 1,500 (green circles) or 10,000 (brown squares) ppm S (Muth and Wallace, 2021).

or more periods of subduction-related metasomatism prior to sub-arc melting, or whether metasomatism (by fluids or silicate melts) and mantle melting happen simultaneously. In the first scenario, there is no clear upper limit to the capacity of S^{6+} to oxidize Fe^{2+} through some combination of porous flow, channelized flow, and/or diapiric ascent of slab material (Spandler and Pirard, 2013). In contrast, a single stage 'direct flux melting' scenario requires a link between the mass transfer of sulfur and associated increases in f_{O2} during mantle melting.

If we assume that during direct flux melting all S^{6+} added to the mantle source remains in mantle melts, we can test how equilibrium between sulfur and iron redox state affects the relationship between slab-derived S^{6+} and arc magma f_{O2}. A highly simplified way to illustrate the coupled redox relationship between sulfur and iron is to 'titrate' S^{6+} into a basaltic melt with the composition of N-MORB (Gale et al., 2013), assuming an initial S^{2-} content of 800 ppm. In this calculation, we use a modified version of the S-Fe redox equilibrium model of Nash et al. (2019) described in the supplement of Muth and Wallace (2021). The results of this simple calculation show that after the first ~1,500 ppm S^{6+} addition to a MORB-like mantle melt, during which the melt becomes increasingly oxidized and S^{6+}-dominated, the S-Fe equilibrium shifts less drastically in response to further S^{6+} addition. This occurs because as the f_{O2} of the melt increases, a given amount of S^{6+} will have a smaller effect on the overall redox budget of the S-Fe redox couple. This smaller shift means that S^{6+} addition becomes less efficient at increasing melt $Fe^{3+}/\Sigma Fe$ and f_{O2} (Fig. 9).

A more realistic simulation of flux melting of the mantle can be achieved by combining these types of redox equilibrium calculations with pMELTS-based mantle melting models. Details of this modelling approach are described in Muth and Wallace (2021). The results of such model calculations show the same decrease in the ability of S^{6+} to oxidize Fe as f_{O2} is increased (Fig. 9; Muth and Wallace, 2021). Therefore, this waning effect of S^{6+} addition during direct flux melting could explain why f_{O2} values across arcs cover a broadly similar range, despite a wide range of slab thermal conditions and primary magma S contents (Fig. 3).

Atypical arc magma compositions provide valuable test cases for the influence of S-Fe redox systematics on arc magma f_{O2}. For example, submarine boninite glasses in the Mariana arc have extremely low (< 200 ppm) sulfur contents but f_{O2} comparable to other arc magmas (Brounce et al., 2021). Low sulfur could be caused by degassing during eruption at the sea floor. Alternatively, these low sulfur contents may result from large degrees of melting of an extremely depleted ambient mantle source. If the latter source-based model is accurate, elevated f_{O2} in boninites could be caused by S^{6+} addition to the mantle wedge even though melt sulfur concentration becomes diluted during mantle melting. Elevated f_{O2} may also partially reflect the increased efficiency of S^{6+} oxidation in mantle sources where all sulfides have been previously extracted (Muth and Wallace, 2021).

4.3. Implications for the Cu contents of mafic arc magmas

Cu and other chalcophile elements partition strongly into magmatic sulfides and are therefore sensitive to the amount of sulfide present during mantle melting and crystallization (Lee et al., 2012; Richards, 2015; Yao et al., 2018). Arc magmas show a wide range of Cu behavior during crystallization, and the cause of this variability is debated (e.g., Rezeau and Jagoutz, 2020; Barber et al., 2021; Park et al., 2021; and references therein). The behavior of sulfur and copper during melting in the sub-arc mantle is also the subject of debate. During mantle melting, melts generated in more oxidizing conditions carry more sulfur and therefore the amount of residual sulfide in the mantle source decreases at constant extent of melting as f_{O2} is increased. This causes more Cu to dissolve

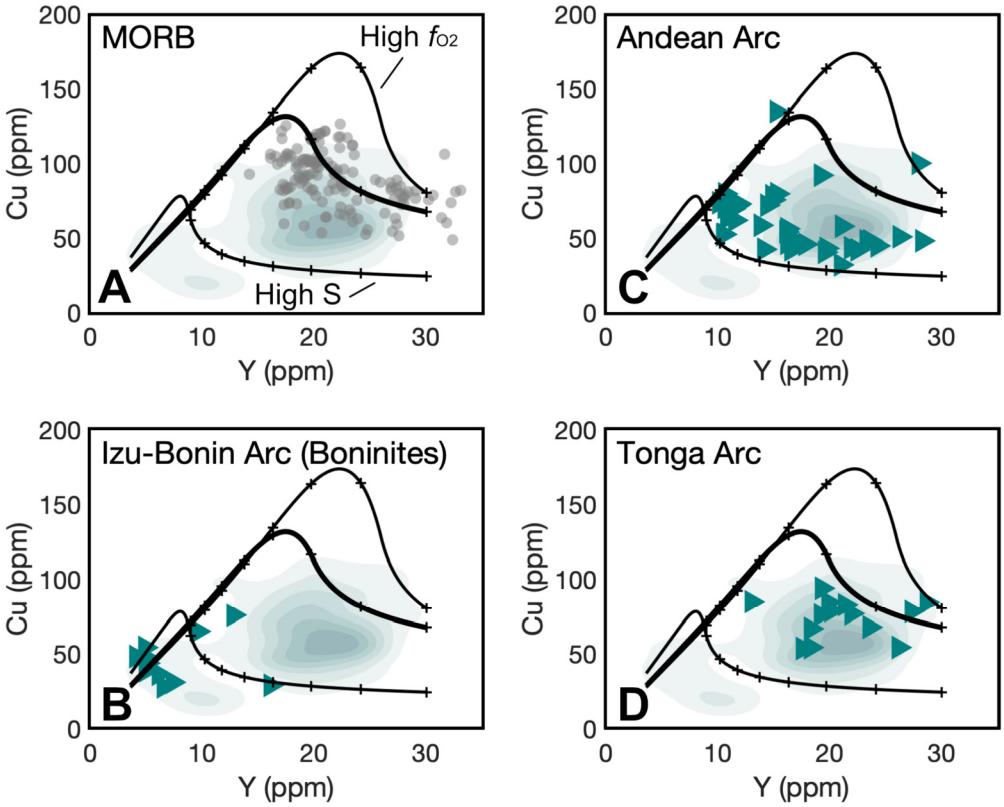

Fig. 10. Primary magma Cu contents from arcs globally (teal density contour), individual arc segments (teal triangles), and MORB (gray circles; Jenner and O'Neil, 2012). All data are filtered to only include primitive (MgO > 10 wt. %) compositions. Black curves represent near aggregate melting models modified from Lee et al. (2012) at 1.1 GPa and 1320 °C assuming 25 ppm Cu and 3.33 ppm Y in the mantle source. Thick curves represent models run assuming 170 ppm S in the mantle source after Sun et al. (2020) and assuming sulfur is present only as S^{2-}. Thin curves represent models run assuming either high concentration of sulfur (470 ppm) in the mantle source (lower curve on each panel) or more oxidizing conditions (QFM + 1).

in mantle melts under more oxidizing conditions. However, despite strong evidence for oxidizing conditions during arc magma generation, the Cu contents of primitive arc magmas globally are overall similar to MORB Cu contents (Lee et al., 2012; Zhao et al., 2022). Global compilations of primitive arc magmas suggest some variations between volcanic arcs within a generally MORB-like range (Zhang et al., 2021; Zhao et al., 2022), potentially related to melt fraction and crustal thickness (Zhao et al., 2022), but the paucity of primitive basalt data in many arcs complicates detailed comparisons. Overall, the similarity in Cu contents between primitive arc magmas and MORB suggests that the mantle sources for both magma types contain similar amounts of sulfide during melting (Lee et al., 2012).

This contradiction can be reconciled by considering the role of slab-derived sulfur during arc magma generation. Whereas oxidizing conditions can decrease the amount of residual mantle sulfide present during melting, a mantle source with higher sulfur contents will retain a higher modal proportion of mantle sulfide during melting at a given f_{O2} (Fig. 10). This is because in the reducing to moderately oxidizing conditions (i.e. below sulfate saturation) any sulfur present in mantle peridotite is present as sulfide (Chowdhury and Dasgupta, 2019). For arcs, where slab-derived sulfate can cause simultaneous increases in both the oxidation state and sulfur content of the mantle source, these competing effects likely play an important role in moderating melt Cu contents. Variations within the broadly MORB-like Cu contents of primitive arc magmas may be due to variability in how magma f_{O2} increases relative to increases in mantle source sulfur content, which would shift the degree to which each of these factors influenced mantle melt Cu content. Mantle melt fraction may also play a role (Zhao et al., 2022). Interestingly, the low Cu contents of magmas such as boninites that form from extremely depleted mantle sources also suggest that the mantle source Cu content plays a role. Overall, these calculations demonstrate that oxidized, slab-derived sulfur can explain the MORB-like Cu contents of arc magmas, consistent with other recent interpretations (Zhao et al., 2022). Considering slab-derived sulfur also raises the possibility that slab components transfer Cu from the slab into the wedge (e.g., Walters et al., 2021), but that in most settings this transfer is masked by the increased amount of S.

Although the addition of slab-derived materials does not strongly increase the Cu contents of arc magmas, slab-derived materials can still play an important role in the generation of porphyry Cu deposits. Magmas associated with fertile porphyry Cu deposits have high Sr/Y signatures (Park et al., 2021). In our compilation, we observe that Sr/Y and S/Dy ratios correlate in arc basalts (Fig. 6). We also show that higher sulfur contents correlate with greater magma oxidation state. These observations fit in well with current conceptual models of crustal processes. High-sulfur, oxidized magmas are more likely to precipitate anhydrite during crustal storage, providing an easily remobilized source of sulfur in crustal magma reservoirs (Chambefort et al., 2008). Magmas strongly influenced by slab components are also likely to have high H_2O contents, which can also promote the development of porphyry deposits (Rezeau and Jagoutz, 2020).

5. Conclusions

We have compiled olivine-hosted melt inclusion compositional data from 140 volcanoes in 32 subduction zone segments and have used this data to estimate primary magma sulfur contents at each volcano. We find that sulfur concentrations in primary magmas

from each arc range from 466 ± 220 ppm to 4,264 ± 819 ppm. Melt S/Dy does not correlate with indicators of mantle depletion such as Nb/Y, showing that the enrichment or depletion of the mantle source before the addition of subduction-derived components is not a strong control on magma S concentration. Instead, S/Dy correlates with proxies for slab-derived components such as ΔTh/Yb. We conclude from these observations that addition of slab-derived sulfur plays an important role in determining the sulfur contents of arc magmas. To quantify the role of oxygen fugacity in controlling arc magma sulfur concentrations, we calculate the minimum f_{O2} needed to match the sulfur contents of primary magmas from each volcano. We find that 88% of primary arc magmas require f_{O2} greater than QFM, and the data require minimum relative f_{O2} values up to QFM + 1.5. Correlations between S/Dy and relative f_{O2} suggest slab-derived S and f_{O2} are related. The upper limit for relative f_{O2} values in arc magmas is likely caused by S-Fe redox interactions during flux melting of the mantle wedge.

Identifying the influence of slab-derived sulfur and associated increases in arc magma f_{O2} globally allows us to tether the consideration of sulfur to a broader understanding of subduction zone processes. The mass transfer of sulfur from the slab can maintain sulfide saturation in the sub-arc mantle wedge even in relatively oxidizing conditions and can thus reconcile the MORB-like Cu contents of arc magmas with evidence reported here and elsewhere for oxidizing conditions during sub-arc mantle melting. High Sr/Y ratios are correlated with high-S, oxidizing magmas, and this relationship can partially explain the association between high Sr/Y magmas and the formation of porphyry Cu deposits.

CRediT authorship contribution statement

Michelle Muth: Conceptualization, Data Curation and Synthesis, Modelling, Writing – Original Draft. **Paul Wallace**: Conceptualization, Input on Data Curation and Synthesis, Writing – Review and Editing.

Declaration of competing interest

The authors declare that they have no known competing financial interests or personal relationships that could have appeared to influence the work reported in this paper.

Data availability

The data and code used in this paper are included in the supplemental materials.

Acknowledgements

This material is based upon work supported by the U.S. National Science Foundation (NSF) Graduate Research Fellowship under grant 1842486. We thank Nicholas Barber, Jesse Walters, and Katie Kelley for thoughtful and constructive reviews.

Appendix A. Supplementary material

Supplementary material related to this article can be found online at https://doi.org/10.1016/j.epsl.2022.117836.

References

Ague, J.J., Tassara, S., Holycross, M.E., Li, J-L., Cottrell, E., Schwarzenback, E.M., Fassoulas, C., John, T., 2022. Slab-derived devolatilization fluids oxidized by subducted metasedimentary rocks. Nat. Geosci. 15, 320–326.

Alt, J.C., Burdett, J.W., 1992. Sulfur in Pacific deep sea sediments (Leg 129) and implications for cycling of sediment in subduction zones. Proc. Ocean Drill. Program Sci. Results 129.

Alt, J.C., 1995. Sulfur isotopic profile through the oceanic crust: sulfur mobility and seawater-crustal sulfur exchange during hydrothermal alteration. Geology 23, 585–588.

Alt, J.C., Schwarzenbach, E.M., Früh-Green, G.L., Shanks, W.C., Bernasconi, S.M., Garrido, C.J., Crispini, L., Gaggero, L., Padrón-Navarta, J.A., Marchesi, C., 2013. The role of serpentinites in cycling of carbon and sulfur: seafloor serpentinization and subduction metamorphism. Lithos 178, 40–54.

Barber, N.D., Edmonds, M., Jenner, F., Audétat, A., Williams, H., 2021. Amphibole control on copper systematics in arcs: insights from the analysis of global datasets. Geochim. Cosmochim. Acta 307, 192–211.

Bénard, A., Klimm, K., Woodland, A.B., Arculus, R.J., Wilke, M., Botcharnikov, R.E., Shimizu, N., Nebel, O., Rivard, C., Ionov, D.A., 2018. Oxidising agents in sub-arc mantle melts link slab devolatilisation and arc magmas. Nat. Commun. 9, 3500.

Botcharnikov, R.E., Linnen, R.L., Wilke, M., Holtz, F., Jugo, P.J., Berndt, J., 2011. High gold concentrations in sulphide-bearing magma under oxidizing conditions. Nat. Geosci. 4, 112–115.

Brounce, M., Reagan, M.K., Kelley, K.A., Cottrell, E., Shimizu, K., Almeev, R., 2021. Covariation of slab tracers, volatiles, and oxidation during subduction initiation. Geochem. Geophys. Geosyst. 22, e2021GC009823.

Callegaro, S., Geraki, K., Marzoli, A., de Min, A., Maneta, V., Baker, D.R., 2020. The quintet completed: the partitioning of sulfur between nominally volatile-free minerals and silicate melts. Am. Mineral. 105, 697–707.

Canil, D., Fellows, S.A., 2017. Sulphide–sulphate stability and melting in subducted sediment and its role in arc mantle redox and chalcophile cycling in space and time. Earth Planet. Sci. Lett. 470, 73–86.

Carroll, M.R., Rutherford, M.J., 1987. The stability of igneous anhydrite: experimental results and implications for sulfur behavior in the 1982 El chichon trachyandesite and other evolved magmas. J. Petrol. 28, 781–801.

Cottrell, E., Birner, S., Brounce, M., David, F., Waters, L.E., Kelley, K.A., 2021. Oxygen fugacity across tectonic settings. In: Neuville, D.R., Moretti, R. (Eds.), AGU Geophysical Monograph Redox: Variables and Mechanisms in Magmatism and Volcanism.

Chambefort, I., Dilles, J.H., Kent, A.J.R., 2008. Anhydrite-bearing andesite and dacite as a source for sulfur in magmatic-hydrothermal mineral deposits. Geology 36, 719–722.

Chowdhury, P., Dasgupta, R., 2019. Effect of sulfate on the basaltic liquidus and Sulfur Concentration at Anhydrite Saturation (SCAS) of hydrous basalts – implications for sulfur cycle in subduction zones. Chem. Geol. 522, 162–174.

De Astis, G., Ventura, G., Vilardo, G., 2003. Geodynamic significance of the Aeolian volcanism (Southern Tyrrhenian Sea, Italy) in light of structural, seismological and geochemical data. Tectonics 22, 1–17.

de Moor, J.M., Fischer, T.P., Sharp, Z.D., King, P.L., Wilke, M., Botcharnikov, R.E., Cottrell, E., Zelenski, M., Marty, B., Klimm, K., Rivard, C., Ayalew, D., Ramirez, C., Kelley, K.A., 2013. Sulfur degassing at Erta Ale (Ethiopia) and Masaya (Nicaragua) volcanoes: implications for degassing processes and oxygen fugacities of basaltic systems. Geochem. Geophys. Geosyst. 14 (10), 4076–4108.

de Moor, J.M., Fischer, T.P., Plank, T., 2021. Constraints on the sulfur subduction cycle in Central America from sulfur isotope compositions of volcanic gases. Chem. Geol.

Ding, S., Dasgupta, R., 2017. The fate of sulfide during decompression melting of peridotite – implications for sulfur inventory of the MORB-source depleted upper mantle. Earth Planet. Sci. Lett. 459, 183–195.

Ding, S., Dasgupta, R., 2018. Sulfur inventory of ocean island basalt source regions constrained by modeling the fate of sulfide during decompression melting of a heterogeneous mantle. J. Petrol. 59, 1281–1308.

Evans, K.A., 2012. The redox budget of subduction zones. Earth-Sci. Rev. 113, 11–32.

Evans, K.A., Frost, B.R., 2021. Deserpentinization in subduction zones as a source of oxidation in arcs: a reality check. J. Petrol. 62, 3.

Gale, A., Dalton, C.A., Langmuir, C.H., Su, Y., Schilling, J.G., 2013. The mean composition of ocean ridge basalts. Geochem. Geophys. Geosyst. 14, 489–518.

Georgatou, A., Chiaradia, M., Rezeau, H., Wälle, M., 2018. Magmatic sulphides in Quaternary Ecuadorian arc magmas. Lithos 296–299, 580–599.

Green, T.H., 1994. Experimental studies of trace-element partitioning applicable to igneous petrogenesis. Sedona 16 years later. Chem. Geol. 117, 1–36.

Jégo, S., Dasgupta, R., 2014. The fate of sulfur during fluid-present melting of subducting basaltic crust at variable oxygen fugacity. J. Petrol. 55, 1019–1050.

Jenner, F.E., O'Neil, H.St.C., 2012. Analysis of 60 elements in 616 ocean floor basaltic glasses. Geochem. Geophys. Geosyst. 13.

Jugo, P.J., Luth, R.W., Richards, J., 2005. An experimental study of the sulfur content in basaltic melts saturated with immiscible sulfide or sulfate liquids at 1300 °C and 1.0 GPa. J. Petrol. 46 (4), 783–798.

Jugo, P.J., 2009. Sulfur content at sulfide saturation in oxidized magmas. Geology 37 (5), 415–418.

Jugo, P.J., Wilke, M., Botcharnikov, R.E., 2010. Sulfur K-edge XANES analysis of natural and synthetic basaltic glasses: implications for S speciation and S content as function of oxygen fugacity. Geochim. Cosmochim. Acta 74, 5926–5938.

Kelley, K.A., Cottrell, E., 2009. Water and the oxidation state of subduction zone magmas. Science 325 (80), 605–607.

Kelley, K.A., Cottrell, E., 2012. The influence of magmatic differentiation on the oxidation state of Fe in a basaltic arc magma. Earth Planet. Sci. Lett. 329–330, 109–121.

Klimm, K., Kohn, S.C., Botcharnikov, R.E., 2012. The dissolution mechanism of sulphur in hydrous silicate melts. II: solubility and speciation of sulphur in hydrous silicate melts as a function of f_{O2}. Chem. Geol. 322–323, 250–257.
Lee, C.T.A., Luffi, P., Chin, E.J., Bouchet, R., Dasgupta, R., Morton, D.M., Le Roux, V., Yin, Q.Z., Jin, D., 2012. Copper systematics in arc magmas and implications for crust-mantle differentiation. Science 336, 64–66.
Le Voyer, M., Hauri, E.H., Cottrell, E., Kelley, K.A., Salters, V.J., Langmuir, C.H., Hilton, D.R., Barry, P.H., Füri, E., 2019. Carbon fluxes and primary magma CO_2 contents along the global mid-ocean ridge system. Geochem. Geophys. Geosyst. 20, 1387–1424.
Li, J.L., Schwarzenbach, E.M., John, T., Ague, J.J., Huang, F., Gao, J., Klemd, R., Whitehouse, M.J., Wang, X.S., 2020. Uncovering and quantifying the subduction zone sulfur cycle from the slab perspective. Nat. Commun. 11, 1–12.
Liu, K., Zhang, L., Guo, X., Ni, H., 2021. Effects of sulfide composition and melt H_2O on sulfur content at sulfide saturation in basaltic melts. Chem. Geol. 559, 119913.
Lorand, J.P., Luguet, A., 2016. Chalcophile and siderophile elements in mantle rocks: trace elements controlled by trace minerals. Rev. Mineral. Geochem. 81, 441–488.
Matjuschkin, V., Blundy, J.D., Brooker, R.A., 2016. The effect of pressure on sulphur speciation in mid- to deep-crustal arc magmas and implications for the formation of porphyry copper deposits. Contrib. Mineral. Petrol. 171.
Médard, E., Grove, T.L., 2008. The effect of H_2O on the olivine liquidus of basaltic melts: experiments and thermodynamic models. Contrib. Mineral. Petrol. 155, 417–432.
Mironov, N.L., Portnyagin, M.V., 2018. Coupling of redox conditions of mantle melting and copper and sulfur contents in primary magmas of the Tolbachinsky Dol (Kamchatka) and Juan de Fuca Ridge (Pacific Ocean). Petrology 26 (2), 145–166.
Muth, M.J., Wallace, P.J., 2021. Slab-derived sulfate generates oxidized basaltic magmas in the southern Cascade arc (California, USA). Geology.
Nash, W.M., Smythe, D.J., Wood, B.J., 2019. Compositional and temperature effects on sulfur speciation and solubility in silicate melts. Earth Planet. Sci. Lett. 507, 187–198.
Newton, R.C., Manning, C.E., 2005. Solubility of anhydrite, $CaSO_4$, in NaCl – H_2O solutions at high pressures and temperatures: applications to gluid – rock interaction. J. Petrol. 46, 701–716.
O'Neill, H.St.C., 2021. Comment on "Compositional and temperature effects on sulfur speciation and solubility in silicate melts" by Nash et al. [Earth Planet. Sci. Lett. 507 (2019) 187–198]. Earth Planet. Sci. Lett. 560, 116843.
O'Neill, H.St.C., Mavrogenes, J.A., 2022. The sulfate capacities of silicate melts. Geochim. Cosmochim. Acta.
Park, J-W., Campbell, I.H., Chiaradia, M., Hongda, H., Lee, C-T., 2021. Crustal magmatic controls on the formation of porphyry copper deposits. Nat. Rev. Earth Environ. 2, 542–556.
Pearce, J.A., Peate, D.W., 1995. Tectonic implications of the composition of volcanic arc magmas. Annu. Rev. Earth Planet. Sci. 23, 251–258.
Rezeau, H., Jagoutz, O., 2020. The importance of H_2O in arc magmas for the formation of porphyry Cu deposits. Ore Geol. Rev. 126, 103744.
Richards, J.P., 2015. The oxidation state, and sulfur and Cu contents of arc magmas: implications for metallogeny. Lithos 233, 27–45.
Ruscitto, D.M., Wallace, P.J., Cooper, L.B., Plank, T., 2012. Global variations in H_2O/Ce: 2. Relationships to arc magma geochemistry and volatile fluxes. Geochem. Geophys. Geosyst. 13.
Shimizu, K., Saal, A.E., Myers, C.E., Nagle, A.N., Hauri, E.H., Forsyth, D.W., Kamenetsky, V.S., Niu, Y., 2016. Two-component mantle melting-mixing model for the generation of mid-ocean ridge basalts: implications for the volatile content of the Pacific upper mantle. Geochim. Cosmochim. Acta 176, 44–80.
Smythe, D.J., Wood, B.J., Kiseeva, E.S., 2017. The S content of silicate melts at sulfide saturation: new experiments and a model incorporating the effects of sulfide composition. Am. Mineral. 102, 795–803.
Spandler, C., Pirard, C., 2013. Element recycling from subducting slabs to arc crust: a review. Lithos 170–171, 208–223.
Sugawara, T., 2000. Empirical relationships between temperature, pressure, and MgO content in olivine and pyroxene saturated liquid. J. Geophys. Res. 105 (B4), 8457–8472.
Sun, Z., Xiong, X., Wang, J., Liu, X., Li, L., Ruan, M., Zhang, L., Takahashi, E., 2020. Sulfur abundance and heterogeneity in the MORB mantle estimated by copper partitioning and sulfur solubility modelling. Earth Planet. Sci. Lett. 538.
Syracuse, E.M., van Keken, P.E., Abers, G.A., Suetsugu, D., Bina, C., Inoue, T., Wiens, D., Jellinek, M., 2010. The global range of subduction zone thermal models. Phys. Earth Planet. Inter. 183, 73–90.
Tomkins, A.G., Evans, K.A., 2015. Separate zones of sulfate and sulfide release from subducted mafic oceanic crust. Earth Planet. Sci. Lett. 428, 73–83.
Turner, S.J., Langmuir, C.H., 2022. An evaluation of five models of arc volcanism. J. Petrol. 63 (3), egac010.
Wallace, P.J., Edmonds, M., 2011. The sulfur budget in magmas: evidence from melt inclusions, submarine glasses, and volcanic gas emissions. Rev. Mineral. Geochem. 73, 215–246.
Walowski, K.J., Wallace, P.J., Clynne, M.A., Rasmussen, D.J., Weis, D., 2016. Slab melting and magma formation beneath the southern Cascade arc. Earth Planet. Sci. Lett. 446, 100–112.
Walters, J.B., Cruz-Uribe, A.M., Marschall, H.R., 2019. Isotopic compositions of sulfides in exhumed high-pressure terranes: implications for sulfur cycling in subduction zones. Geochem. Geophys. Geosyst. 20, 3347–3374.
Walters, J.B., Cruz-Uribe, A.M., Marschall, H.R., 2020. Sulfur loss from subducted altered oceanic crust and implications for mantle oxidation. Geochem. Perspect. Lett., 36–41.
Walters, J.B., Cruz-Uribe, A.M., Marschall, H.R., Boucher, B., 2021. The role of sulfides in the chalcophile and siderophile element budget of the subducted oceanic crust. Geochim. Cosmochim. Acta 304, 191–215.
Yao, Z., Qin, K., Mungall, J.E., 2018. Tectonic controls on Ni and Cu contents of primary mantle-derived magmas for the formation of magmatic sulfide deposits. Am. Mineral. 103, 1545–1567.
Xu, Z., Li, Y., 2021. The sulfur concentration at anhydrite saturation in silicate melts: implication for sulfur cycle and oxidation state in subduction zones. Geochim. Cosmochim. Acta 306, 98–123.
Zelenski, M., Kamenetsky, V.S., Nekrylov, N., Kontonikas-Charos, A., 2022. High sulfur in primitive arc magmas, its origin and implications. Minerals 12, 37.
Zhang, H.L., Cottrell, E., Solheid, P.A., Kelley, K.A., Hirschmann, M.M., 2018. Determination of $Fe^{3+}/\Sigma Fe$ of XANES basaltic glass standards by Mössbauer spectroscopy and its application to the oxidation state of iron in MORB. Chem. Geol. 479, 166–175.
Zhang, Y., Gazel, E., Gaetani, G.A., Klein, F., 2021. Serpentinite-derived slab fluids control the oxidation state of the sub-arc mantle. Sci. Adv. 7, eabj2515.
Zhao, S-Y., Yang Yan, A., Langmuir, C.H., Zhao, T-P., 2022. Oxidized primary arc magmas: constraints from Cu/Zr systematics in global arc volcanics. Sci. Adv. 8, eabk0718.s.